PLASMA PHYSICS GROUP

Polarization of the Auroral Electrojet

F. V. Coroniti

C. F. Kennel

February, 1972 PPG-112

UNIVERSITY OF CALIFORNIA
LOS ANGELES

ENGINEERING PHYSICS METEOROLOGY

Polarization of the Auroral Electrojet

F. V. Coroniti

C. F. Kennel

February, 1972 PPG-112

This work was partially supported by the Office of Naval Research, Grant #N00014-69-A-0200-4023; the National Science Foundation, Grant #GP-22817; the Atomic Energy Commission, Contract AT(04-3)-34, Project #157; and the National Aeronautics and Space Administration, Contract NGR-05-007-190 and NGR-05-007-116.

Polarization of the Auroral Electrojet

F. V. Coroniti

C. F. Kennel

Abstract

We consider an idealized model of electrojet polarization. Precipitation from the inner edge of the electron plasma sheet creates a density maximum in the auroral oval ionosphere, which in turn leads to Hall and Pedersen conductance maxima. We then assume a uniform westward convection electric field is imposed upon the lower ionosphere previous to polarization. Field-aligned currents must flow into the ionosphere equatorward, and out poleward, of the Hall conductance maximum. As the convection field and ionospheric density increase during substorm growth phase, the field-aligned current densities should eventually reach an instability threshold, beyond which anomalous resistance should produce field-aligned electric fields. The partial blockage of the field-aligned currents produces an equatorward electric field and therefore a partial Cowling conductivity in the lower ionosphere. Rough numerical estimates indicate that the expected field-aligned currents can exceed the stability threshold estimated by Kindel and Kennel (1971); that 1-5 Kv field-aligned potential drops correspond to significant electrojet enhancement; and that the required energy dissipation of field-aligned currents in the topside ionosphere, a few ergs/cm^2-sec column, suggests significant topside modification following auroral breakup.

1.0 Introduction

The growth phase of magnetospheric substorms commences with a southward shift in the interplanetary magnetic field (Fairfield and Cahill, 1966; Nishida, 1968a,b, 1971; Hirshberg and Colburn, 1969; Aubry et al., 1970; Arnoldy, 1971) which intensifies field-cutting at the nose of the magnetosphere and internal magnetospheric convection (Dungey, 1961; Levy et al., 1964; Axford et al., 1965). Mozer and Manka (1971) and Mozer (1971) have observed, preceding breakup in the nightside auroral oval, a gradual buildup of the westward convection electric field, which drives enhanced ionospheric currents (Oguti, 1968; McPherron, 1970).

In the geomagnetic tail the magnetic field increases by as much as 50% during the growth phase (Fairfield and Ness, 1970; Camidge and Rostoker, 1970; Russell et al, 1971; Aubry and McPherron, 1971) and the plasma sheet thins (Hones, 1970; Hones, et al., 1971). Coroniti and Kennel (1971a, b) have argued that these tail changes are consistent with increased flaring of the tail magnetopause due primarily to a reduction in size of the dayside magnetosphere and an increase in tail flux (Aubry et al., 1970). Other consequences of enhanced tail flaring stress are an increase in plasmasheet plasma pressure, and an earthward motion of the tail currents and electron plasma sheet inner edge (Siscoe and Cummings, 1979).

In this paper we investigate the response of the nightside auroral oval to the enhancement of convection and the intensification of electron precipitation from the plasma sheet. For typical growth phase parameters we find that the field-aligned currents which flow into and out of the auroral oval can exceed the threshold for topside ionospheric current instabilities (Kindel and Kennel, 1971). A direct consequence of any resulting topside anomalous resistance to the current flow is that the

ionospheric electric field polarizes into a Cowling current electrojet configuration. The possibility that the electrojet is a Cowling current has been discussed by Fukushima (1969).

We assume that the nightside oval ionospheric plasma density is maintained solely by the precipitation of plasma sheet electrons. The nightside oval is then bounded at its poleward edge by the last closed tail field line and at its equatorward edge by the inner boundary of the electron plasma sheet (Vasyliunas, 1968). In a flaring tail, the plasma sheet pressure decreases with increasing geocentric distance, implying that the electron precipitation heat flux should decrease poleward. When there is convection, electrons are adiabatically compressed and heated as they flow from the plasma sheet into the dipole field; hence the precipitation heat flux should maximize at the equatorward edge of the oval. Since dissociative recombination is the major ion loss mechanism in the lower ionosphere, the ionospheric plasma density is proportional to the square root of the electron heat flux. Hence the ionospheric density and the height-integrated conductivities -- the conductances -- should increase proceeding equatorward, reach a maximum, and then fall off rapidly at the equatorward edge of the auroral oval. Since inward flow raises the mean electron energy, electron precipitation at the equatorward edge of the oval should penetrate to deeper atmospheric layers (Rees, 1963). Hence the ratio of Hall to Pedersen conductance should maximize there as well.

During growth phase the observed predominantly westward electric field near midnight drives a westward Pedersen and a poleward Hall current. Pedersen currents are never divergence-free in the ionosphere, and must be fed by field-aligned currents into the ionosphere on the morning side and out on the evening side. The north-south gradient of the Hall conductance implies that the poleward Hall current also cannot be divergence-free in the ionosphere, and must therefore be fed by field-aligned currents into the ionosphere at the

equatorward edge, and by outward currents polewards of the maximum of the auroral oval ion density (for a general discussion see Heppner, et al., 1971). Considerations of symmetry suggest that the Pedersen current, and therefore the electric field, ought to maximize in the local midnight sector; hence the poleward Hall current should also maximize near midnight. The field-aligned current density feeding the Hall current will maximize in the region of sharpest north-south gradient of Hall conductance which, upon mapping the sharp inner boundary of the electron plasma sheet into the ionosphere (Vasyliunas, 1968), occurs at the equatorward edge of the oval. The above arguments, together with the facts that east-west ionospheric scale lengths are longer than the north-south, and that the Hall conductance is ordinarily larger than the Pedersen conductance, indicate that the maximum field-aligned current density should be found at the equatorward edge of the auroral oval in the midnight sector.

The build-up of the convection electric field coupled with the enhanced Hall conductance from increased electron precipitation indicates that the field-aligned currents should intensify during substorm growth phase. Since the conductivity parallel to the magnetic field is ordinarily quite large, the field-aligned currents feeding the auroral oval ordinarily flow freely, i.e., without large parallel potential drops. They may have been observed as transverse magnetic perturbations at 1100 km over the auroral oval (Zmuda, et al., 1967; 1970) and as east-west magnetic field perturbations near the boundaries of the plasma sheet by Russell et al. (1971). Field-aligned currents probably also flow in and out along the system of homogeneous arcs often found during growth phase. In this paper, we will conceptually average over such arc systems and consider only the large scale features of the auroral oval current and electric field distribution, a limitation suited to comparison with Mozer's electric field measurements.

The ability of the magnetic field lines to carry parallel currents is not unlimited. According to Kindel and Kennel (1971) parallel current densities of a few times 10^9 electrons $cm^{-2}sec^{-1}$ will lead to electrostatic wave instabilities in the topside ionosphere, generally above 1000 km altitude. The above arguments indicate that as the growth phase develops, a field line near the equatorward edge of the auroral oval in the local midnight sector would be most likely to go unstable first. The nonlinear saturation of current-driven instabilities leads to an "anomalous" parallel resistance, and therefore, the development of parallel electric fields. Then, the field-aligned currents feeding the auroral oval Hall current would be partially blocked. The lower ionosphere must then polarize, creating an equatorward electric field whose Pedersen current reduces the net poleward current in the lower ionosphere. According to Mozer (1971), such an equatorward electric field shift is a characteristic feature of auroral breakup. The equatorward polarization field, equivalent to a partial Cowling conductance, can then strongly enhance the Westward current, when the Hall conductance exceeds the Pedersen conductance.

Thus, following the strict logic of the growth phase development, we have arrived at a salient feature of substorm breakup: an equatorward electric field shift, and an enhancement of the auroral electrojet. However, we have left a "chicken-egg" cause and effect relationship unresolved, since anything in the geomagnetic tail which suddenly enhances earthward convection, would also, by the above logic, polarize the auroral oval ionosphere. In effect, it is unclear whether tail magnetic field collapse causes electrojet polarization, or whether the change in convection boundary conditions implied by electrojet polarization triggers the tail field collapse.

In Section 2.0, we undertake a simplified analysis of electrojet polarization. We assume the auroral oval density enhancement to be uniform between sharp boundaries at the poleward and equatorward edges; field-aligned currents

then flow only at the edges of the oval. We assume a primary quasi-constant westward electric field imposed on the ionosphere by magnetospheric convection. If the convection electric field has a quasi-steady north-south component, then the auroral oval density enhancement should be rotated to be aligned perpendicular to the flow direction. We further assume that any polarization electric field, which results from field-aligned resistance, appears only in the ionosphere below the anomalous resistance region and does not map into the magnetosphere. For steady, sub-sonic convection this assumption is reasonable since the hot magnetospheric plasma will tend to discharge only polarization fields in space. However, for unsteady or rapid flows, the field line capacitance and inductance may permit a polarization electric field to be established in the magnetosphere. With these assumptions the entire lower ionosphere is treated as a lumped element in a circuit comprising the poleward Hall current, the field-aligned currents which flow through resistors, and the currents which arise from the polarization electric field. We then compute the parallel resistance for which the southward polarization and convection field components are roughly equal, corresponding to Mozer's observations at breakup. Field-aligned potential drops of 5 to 10% of the east-west convection potential, a few kV, are required. Thus, without solving the difficult nonlinear anomalous resistance problem, we can infer from Mozer's measurements and the present interpretation the required integrated anomalous resistance needed for polarization. It is interesting that the required potential drops are consistent with the energies of electron beams typically observed (Evans, 1968). Direct rocket measurements of parallel electric fields in the lower ionosphere may also be indicative of anomalous field-aligned resistance (Mozer and Bruston, 1967). Since the anomalous Joule heating in the topside amounts to several ergs/cm^2-sec column, we would expect significant changes in topside structure following breakup.

The analysis in Section 2.0 completely neglects all questions of spatial structure of the auroral oval ionosphere. However, the gradient scalelengths determine the field-aligned current density, and therefore, whether or not topside current instabilities are possible. Thus, we must create a model for the north-south ionospheric density profile, which in turn depends upon the profile of electron precipitation. In the absence of parallel electric field, the electron precipitation rate depends upon the electron distribution in space and the pitch angle scattering rate. Only in the limit of strong pitch angle diffusion can the electron precipitation rate be conveniently estimated, a priori. The observed isotropy of the electron precipitation fluxes into the auroral oval suggests they are often near the strong diffusion limit (Kennel, 1969). In Section 3.0, we couple strong diffusion precipitation and convection, following Kennel (1969), to find the spatial profile of the electron precipitation fluxes. Since this profile depends critically upon the magnetic topology, we can uniquely model only the inner edge of the plasma sheet where the convection flow penetrates an essentially dipolar field. The electron heat flux can then be approximately related to the E-region ionospheric density and therefore the Hall and Pedersen conductances. The idealizations involved in this model suggest that it may often err quantitatively; however, we hope no essential physical trends have been overlooked.

In Section 4.0 the effects of parallel resistance are investigated. Here we treat the anomalous resistance as a small perturbation, in the sense that runaway electron beams created by the parallel electric field produce no additional ionization in the lower ionosphere. This is certainly not the case in auroral arcs. However, we hope the large scale structure is adequately treated. We find that typical growth phase ionospheric conductances and electric fields can lead to parallel current densities which exceed the stability threshold. The threshold is exceeded first at the equatorward edge of the auroral oval, and then as the

electric field increases, somewhat further north. The polarization model has a broad region, several hundred kilometers thick, of westward electrojet, which may in fact be divided into two parts. There is a weak eastward electrojet, equatorward of the main westward electrojet.

2.0 Polarization of a Block Ionosphere

We treat the polarization of an idealized two-dimensional auroral oval, in which the conductivity enhancement produced by plasma sheet electron precipitation is sharply bounded at its northern and southern edges and uniform in between. When a uniform westward electric field is applied, field-aligned currents flow into the ionosphere at the southern edge and out at the northern edge. No field-aligned currents flow elsewhere. The field-aligned currents bounding the oval are assumed to produce anomalous parallel resistances which produce a polarization electric field in the lower ionosphere.

Consider a Cartesian coordinate system appropriate to the nightside northern auroral oval, in which z points vertically upwards, x southward, and y eastward. For simplicity, the geomagnetic field is assumed to point in the -z direction. The oval ionosphere is assumed uniform in y, to be sharply bounded at its northern and southern edges, and to be uniform over its north-south width w. The height-integrated currents within the oval then obey

$$I_x = \Sigma_P E_x + \Sigma_H E_y \qquad (2.1a)$$

$$I_y = \Sigma_P E_y - \Sigma_H E_x \qquad (2.1b)$$

where Σ_P and Σ_H denote the (height-integrated) Pedersen and Hall conductances, respectively. For simplicity, we assume that the net Pedersen resistance of the polar cap and sub-auroral regions is sufficiently large that no north-south Pedersen currents can flow outside the oval. Furthermore, we define Δ_S and Δ_N as the difference between the Hall conductivity of the auroral oval and the sub-auroral region, and of the oval and polar cap, respectively. I_x has a divergence in two dimensions which requires field-aligned currents I_S, I_N at the southern and northern edges of the auroral oval respectively.

$$I_S = \sum_P E_x + E_y \Delta_S \tag{2.2a}$$

$$I_N = -\sum_P E_x - \Delta_N E_y \tag{2.2b}$$

Note that if $\Delta_S = \Delta_N$, then $I_S = -I_N$. Furthermore, when the oval is unpolarized ($E_x = 0$), a westward convection field ($E_y < 0$) implies $I_S < 0$, $I_N > 0$, or field-aligned currents in at the southern edge of the oval and out at the northern edge. We now treat the whole auroral oval bottomside ionosphere as an element in a circuit involving the field-aligned currents. We assume that when $|I_S|$, $|I_N|$ exceed certain thresholds, they will go unstable somewhere in the topside ionosphere, and produce integrated anomalous resistances R_S and R_N. Furthermore, we assume that for sub-sonic flow the field line capacitance can be neglected and that any polarization electric field in space is discharged by the hot, highly conducting magnetospheric plasma. Therefore, E_x exists only below the anomalous resistance region. The condition that the potential drops across R_S and R_N just balance the potential across the auroral oval due to any polarization E_x is

$$E_x w = R_N I_N - R_S I_S \tag{2.3}$$

E_y is assumed imposed by magnetospheric convection, and uniform in x. Finally, we define $P = w/\sum_P$, the integrated Pedersen resistance across the auroral oval in the north-south direction, w being the width of the oval.

After some algebra, we arrive at the following relations

$$I_S = E_y \frac{\left[\Delta_S + \frac{R_N}{P}(\Delta_S - \Delta_N)\right]}{1 + (R_S+R_N)/P} \tag{2.4a}$$

$$I_N = -E_y \frac{\left[\Delta_N - \frac{R_S}{P}(\Delta_S - \Delta_N)\right]}{1 + (R_S+R_N)/P} \tag{2.4b}$$

$$I_x = E_y \left[\Sigma_H - \frac{R_S\Delta_S + R_N\Delta_N}{P + R_S + R_N} \right] \tag{2.4c}$$

$$I_y = E_y \left[\Sigma_P + \frac{\Sigma_H}{\Sigma_P} \frac{R_S\Delta_S + R_N\Delta_N}{P + R_S + R_N} \right] \tag{2.4d}$$

$$\frac{E_x}{E_y} = - \frac{1}{\Sigma_P} \frac{R_S\Delta_S + R_N\Delta_N}{P + R_S + R_N} \tag{2.4e}$$

If $\Delta_S = \Delta_N = 0$, corresponding to a completely uniform ionosphere, there are no field-aligned currents ($I_S = I_N = 0$), there is no polarization E_x, and consequently no enhancement of the electrojet, $I_y = \Sigma_P E_y$. Next consider the case where Δ_S, $\Delta_N \neq 0$, but the products $E_y\Delta_S$, $E_y\Delta_N$ do not produce field-aligned currents above the threshold for instability. Then R_S and R_N will be effectively zero. Since the field-aligned currents required to feed the auroral oval Hall current flow freely along field lines between the ionosphere and outer space, there is no polarization E_x and no electrojet enhancement. Finally, we can recover the classical Cowling conductivity, by assuming at least one field-aligned resistance, say R_S, to be very large. In this case,

$$I_S \to 0 \tag{2.5a}$$

$$I_N \to E_y(\Delta_S - \Delta_N) \tag{2.5b}$$

$$I_x \to E_y(\Sigma_H - \Delta_S) \tag{2.5c}$$

$$I_y \to E_y \left[\Sigma_P + \frac{\Sigma_H\Delta_S}{\Sigma_P} \right] \tag{2.5d}$$

$$\frac{E_x}{E_y} \to - \frac{\Delta_S}{\Sigma_P} \tag{2.5e}$$

In the limit $\Delta_S \gtrsim \Sigma_H \gtrsim \Delta_N$, $I_S = I_N = I_x = 0$, $E_x/E_y = -\Sigma_H/\Sigma_P$, $I_y = E_y[\Sigma_P + \Sigma_H^2/\Sigma_P]$. Here the Cowling conductivity provides a strong electrojet when $\Sigma_H/\Sigma_P >> 1$ which is usually the case for the nightside oval (Bostrom, 1964). Clearly, anomalous resistance becomes important, and the transition from Pedersen to Cowling conductivity for the electrojet occurs, when $(R_S + R_N)/P$ grows to be of order one .

Mozer's (1971) electric field measurements indicate that a southward electric field develops during substorm breakup whose magnitude is roughly equal to the original westward electric field. If we interpret the southward field shift as due to the development of anomalous field-aligned resistances, then we may use the observational condition $|E_x/E_y| \sim 1$ to infer several properties of the anomalous resistances without invoking detailed kinetic theory solutions for the saturation of current-driven instabilities in the topside ionosphere. In the discussion to follow, we will assume for simplicity $\Delta = \Delta_S = \Delta_N$, $R_S = R_N = R$.

Let us define $E_x/E_y = -1$ to be polarization onset. This occurs when

$$R = \frac{P/2}{\Delta/\Sigma_P - 1} = \frac{1}{2}\frac{w}{\Sigma_H - \Sigma_P} \tag{2.6}$$

where $\Delta \gtrsim \Sigma_H$.

$E_x/E_y \gtrsim -1$ is only possible if $\Sigma_H > \Sigma_P$. When $\Sigma_H >> \Sigma_P$, polarization occurs when each parallel resistance is roughly equal to half the north-south integrated Hall resistance. For polarization onset, the bottomside currents are given by

$$I_x = (\Delta - \Sigma_P)E_y \quad ; \quad I_y = E_y(\Delta + \Sigma_P) \tag{2.7}$$

Thus, the electrojet is enhanced by a factor $1 + \Delta/\Sigma_P$ relative to the unpolarized state previous to breakup.

The magnitude of the field-aligned potential drops is given by

$$\Delta V_{\parallel} = RI = \frac{|E_y| \Sigma_H R}{1+2R/P} \tag{2.8}$$

which, for polarization onset, reduces to $\Delta V_{\parallel} = \frac{|E_y| w}{2}$. If we estimate $|E_y| = \Phi/\ell$ where Φ is the east-west potential across the auroral oval and ℓ is the length of the auroral oval in the east-west direction, then

$$\frac{\Delta V_{\parallel}}{\Phi} \approx \frac{w}{2\ell} \tag{2.9}$$

Since $w/2\ell \approx 0.05$ to 0.1, a field-aligned potential drop of roughly 5 to 10% the emf along the oval can produce polarization and an electrojet. The total energy dissipation, per unit length, of the field-aligned currents in one resistor at polarization onset is given by

$$\dot{W}_{\parallel} = I^2 R = \frac{|E_y|^2}{2} (\Sigma_H - \Sigma_P) w \tag{2.10}$$

and the ratio of topside to total bottomside energy dissipation, at polarization onset is

$$\frac{\dot{W}_{\parallel}}{\dot{W}_{\perp}} = \frac{\Delta - \Sigma_P}{2\Sigma_P} \tag{2.11}$$

where both parallel resistors have been counted. When $\Delta >> 3\Sigma_P$, more energy is dissipated in parallel than in perpendicular currents.

Let us now insert some characteristic values of the parameters involved in 2.6 - 2.11 to test the plausibility of these estimates. We assume $w \approx 600$ km (a 6° auroral oval) and $\ell \approx 6{,}000$ km (an oval which extends from local evening to local dawn.) Then if the emf Φ at breakup is 120 kV, we find $\Delta V_{\parallel} \approx 6$Kv. Since this is comparable with the characteristic energy of mono-energetic particle beams observed during breakup (Evans, 1968), it does not seem

unreasonable. When $\Delta - \Sigma_P \approx 2 \times 10^{13}$esu = 20 mhos, the dissipation in the two parallel resistors, from 2.10, is 1.6×10^7 ergs/cm-sec, which if the electrojet extends over 6,000 km, amounts to 8×10^{17} ergs/sec in all. If the field-aligned currents are actually distributed, and the energy dissipation $\dot{W}_{\parallel}$ is more or less uniform over the width $w \approx 600$ km, the field-aligned current dissipation per cm^2 column is roughly 2 ergs/cm^2-sec. Such an energy in the low density topside ionosphere should lead to a gross change in its structure at substorm breakup.

Thus, this simple idealized model of electrojet polarization, leads to the following general conclusions. First, when $\Delta/\Sigma_P > 1$, small field-aligned potential drops correspond to significant electrojet enhancements. Secondly, the observation that $|E_x/E_y| \approx 1$ implies that the energy dissipation of field-aligned currents after breakup is comparable to that of the Pedersen currents in the lower ionosphere. Hence significant heating of the topside ionosphere should occur when the electrojet is enhanced by polarization.

3.0 Strong Diffusion Electron Precipitation Profile

Here, we construct a model for the latitudinal distribution of the energetic electrons precipitating from the plasma sheet into the nightside auroral oval ionosphere. We assume that the electron fluxes are maintained nearly isotropic in pitch angle, not an unreasonable assumption since the precipitating electrons are often observed to be isotropic (Kennel, 1969). By combining strong diffusion precipitation with convection, a spatial profile of electron precipitation may be deduced. This profile depends strongly on the magnetic field topology, which can only be uniquely specified for the inner edge of the plasma sheet where convection carries the plasma sheet electrons into a more or less dipolar field.

A solution for the penetration hot precipitating electrons into a dipole field has been obtained by Kennel (1969)

$$\frac{n(L)}{n(L_T)} \cong \left(\frac{L_T}{L}\right)^4 \exp\left\{-\frac{3\delta}{22}\left[\left(\frac{L_T}{L}\right)^{22/3} - 1\right]\right\} \quad L < L_T \qquad (3.1)$$

where $n(L)$ is the electron density, L denotes the L-shell and L_T denotes the largest L-parameter in the magnetic midnight meridian plane where the magnetic field may reasonably be considered dipolar. (3.1) is restricted to the magnetic midnight meridian; L_T, which may be estimated using the procedure of Siscoe and Cummings (1969), is typically 8-10, depending upon the strength of the geomagnetic tail field. The parameter δ describes the relative strength of convection and strong diffusion electron precipitation:

$$\delta = \frac{L_T}{\tilde{L}} \quad ; \quad \tilde{L} = \frac{CE}{B} T_{min}\Big|_{L = L_T} \qquad (3.2)$$

where E is the convection field, assumed westward and constant in space and time in the equatorial plane; CE/B is the equatorial plane convection speed, and T_{min} is the electron minimum lifetime. For a dipole field, the electron minimum lifetime is roughly $L^4/\sqrt{E_e(keV)}$ seconds, Rather than consider the variation of T_{min} with energy E_e, the above solution assumes that electrons are lost on a characteristic timescale equal to the minimum lifetime of an electron at the thermal energy; i.e. $T_{min} = L^4/\sqrt{T_e(keV)}$. For an adiabatic gas with $\gamma = 5/3$ (appropriate to pitch angle isotropy with small precipitation losses) T_e scales as

$$\frac{T_e(L)}{T_e(L_T)} = \left(\frac{L_T}{L}\right)^{4\gamma-4} = \left(\frac{L_T}{L}\right)^{8/3} \tag{3.3}$$

(3.3) should be approximately valid until the flow carries the plasma beyond the density maximum, at which point precipitation energy losses become significant. The maximum of n(L) occurs at $L/L_T = (\delta/4)^{3/22}$; the maximum hot electron density, n^*, is

$$\frac{n^*}{n(L_T)} = \left(\frac{4}{\delta}\right)^{6/11} \exp\left\{+\frac{3\delta}{22} - 6/11\right\} \tag{3.4}$$

Within $L < L_T(\delta/4)^{3/22}$, n decreases rapidly; this region of decrease is the inner edge of the electron plasma sheet. When the electron precipitation flux exceeds the proton precipitation flux, a return current of cold electrons must flow from the ionosphere to maintain charge neutrality. Vasyliunas (1968) has suggested that the cold and hot electrons mix in less than a flow time, thereby lowering the hot electron temperature. This effect has not been included here; it would weaken the gradient of hot electron density at the inner edge, and decrease the electron temperature. Two other quantities of

interest are the omnidirection particle flux J, which is twice the precipitation flux, and the electron precipitation heat flux, F. For Maxwellian energy distributions, these would scale as

$$J = \frac{n}{4}\sqrt{\frac{T_e}{m_e}} \tag{3.5}$$

$$F = \sqrt{\frac{8}{\pi m_e}}\, n_e\, T_e^{3/2}$$

where m_e is the electron mass. We will use these scalings as illustrations.

Inserting (3.1) and (3.3) into (3.5), we arrive at

$$\frac{J(L)}{J(L_T)} = \left(\frac{L_T}{L}\right)^{16/3} \exp\left\{\frac{-3\delta}{22}\left[\left(\frac{L_T}{L}\right)^{22/3} - 1\right]\right\} \tag{3.6a}$$

$$\frac{F(L)}{F(L_T)} = \left(\frac{L_T}{L}\right)^{8} \exp\left\{-\frac{3\delta}{22}\left[\left(\frac{L_T}{L}\right)^{22/3} - 1\right]\right\} \tag{3.6b}$$

J and F have maxima at $(L/L_T) = \left(\frac{3\delta}{16}\right)^{3/22}$ and $(\delta/8)^{3/22}$ respectively; the magnitudes of the maxima are given by

$$\frac{J^*}{J(L_T)} = \left(\frac{16}{3\delta}\right)^{8/11} \exp\left\{\frac{3\delta}{22} - 8/11\right\} \tag{3.7a}$$

$$\frac{F^*}{F(L_T)} = (8/\delta)^{12/11} \exp\left\{\frac{3\delta}{22} - 12/11\right\} \tag{3.7b}$$

The electron temperature at the heat flux maximum is given by $T_e^* = T_e(L_T) \cdot (8/\delta)^{4/11}$. The maxima of the successively higher moments fall increasingly close to the Earth because of convection plasma heating, here undiluted by mixing with cold ionospheric plasma. Furthermore, since $\delta \propto E^{-1}$, the successively higher moments have maxima whose magnitudes are increasingly strong functions

of E. In particular, the maximum heat flux varies approximately as the convection electric field. Thus, due to betatron heating, convection enhancements significantly increase the electron energy deposited in the auroral oval ionosphere. However, the locations of the hot number density, flux, and heat flux maxima are weakly dependent upon E, varying as $E^{-3/22}$. Thus, equatorward motions of the auroral oval are primarily due to decreases in L_T caused by increasing geomagnetic tail fields.

The above solutions may be mapped onto the auroral oval ionosphere, using the relation

$$\frac{\sin^2\theta_T}{\sin^2\theta} \approx \frac{\theta_T^2}{\theta^2} \approx \frac{x_T^2}{x^2} = \frac{L}{L_T} \tag{3.8}$$

where θ is the magnetic colatitude, θ_T the colatitude corresponding to the last dipolar tube of force, $L = L_T$. $x = R_E\theta$ is the linear distance from the geomagnetic pole in the midnight meridian plane. The approximation $\theta << 1$ is reasonably accurate for $L > 6$. From (3.8), the heat flux F(L) maps as

$$\frac{F(x)}{F(x_T)} = \left(\frac{x}{x_T}\right)^{16} \exp\left\{-\frac{3\delta}{22}\left[\left(\frac{x}{x_T}\right)^{44/3} - 1\right]\right\} \tag{3.9}$$

4.0 Polarization of Auroral Oval Ionosphere

4.1 Basic Equations

Let us assume the conducting E-region of the ionosphere has an effective height h, denote the mean electron and ion densities by N_e and N_i respectively, and the field-aligned current density above the E-region by $j_{\parallel}$. Then rough equations for N_e and N_i may be constructed:

$$\frac{\partial N_e}{\partial t} + \frac{\partial}{\partial x}(N_e V_{D_e}) + \alpha N_e^2 = \frac{F(x)}{kh} + \frac{j_{\parallel}}{eh} \tag{4.1a}$$

$$\frac{\partial N_i}{\partial t} + \frac{\partial}{\partial x}(N_i V_{D_i}) + \alpha N_i^2 = \frac{F(x)}{kh} \tag{4.1b}$$

where V_{D_e}, V_{D_i} are the electron and ion drifts in the north-south (x) direction, and east-west spatial gradients have been neglected. α is a volume dissociative recombination coefficient, F is the electron precipitation heat flux, and K = 35 eV/ion pair, the ionization efficiency. $j_{\parallel}$ has been assumed to be carried completely by electrons. Furthermore,we assume that runaway electrons, accelerated by a field-aligned potential, do not carry any of the parallel current, so that $j_{\parallel}$ does not ionize the lower ionosphere.

We define the height-integrated current I_x to be roughly $I_x = N_i eh(V_{D_i} - V_{D_e})$ where charge neutrality has been assumed. The subtracting (4.1a) from (4.1b), we arrive at a current continuity equation

$$\frac{\partial I_x}{\partial x} = -j_{\parallel} \tag{4.2}$$

We may relate I_x to the perpendicular electric fields by the conductivity law

$$I_x = \Sigma_P E_x + \Sigma_H E_y \equiv N[PE_x + HE_y] \tag{4.3}$$

where in the second form of (4.3), the Pedersen and Hall conductances have been assumed proportional to the mean E-region ionospheric density.

Henceforth, E_y, the convection field, will be assumed given, and E_x to arise from polarization created by field-aligned potential drops in the topside ionosphere. Since the electric field in the ionosphere is curl-free to a very good approximation, we have $\frac{\partial E_x}{\partial z} = \frac{\partial E_z}{\partial x}$. Then defining $\underline{E} = -\underset{\sim}{\nabla}\phi$, $\phi_{\shortparallel} \simeq -\int_{z_1}^{\infty} E_z dz$ where z_1 denotes the top of the E-region, and integrating

$$\int_{z_1}^{\infty} \frac{\partial E_x}{\partial z}\, dz = E_x(\infty) - E_x(z_1) = \frac{\partial}{\partial x}\int_{z_1}^{\infty} E_z dz = -\frac{\partial \phi_{\shortparallel}}{\partial x} \tag{4.4}$$

Then, again assuming that no polarization E_x exists in the magnetosphere so that $E_x(\infty) = 0$, we arrive at a relation between the polarization field in the lower ionosphere and the field-aligned potential drop

$$E_x = \frac{\partial \phi_{\shortparallel}}{\partial x} \tag{4.5}$$

We now construct a simplified model for the effects of anomalous resistance. We expect $E_{\shortparallel} = \eta j_{\shortparallel}$ where η is the anomalous resistance. Similarly, since $E_{\shortparallel} = -\partial\phi_{\shortparallel}/\partial z$ we also expect

$$\phi_{\shortparallel} = -r(x) j_{\shortparallel} \tag{4.6}$$

where $r(x)$ is the height-integrated resistance. In general, r will depend upon $|j_{\shortparallel}|$. For example, the results of Kindel and Kennel (1971) indicate that r will remain zero until $|j_{\shortparallel}|$ exceeds a certain threshold of order 3×10^9 e/cm^2-sec. Similarly, the laboratory results of Hamberger and Jancarik (1972) indicate that r increases significantly each time $|j_{\shortparallel}|$ increases to exceed the threshold of a stronger current instability, for example, the

transition from ion acoustic to electron-ion beam instability.

Combining (4.5) and (4.6), we find

$$E_x = - \frac{\partial}{\partial x} (r j_{\shortparallel}) \tag{4.7}$$

and using (4.2),

$$E_x = \partial/\partial x \ (r \frac{\partial I_x}{\partial x}) \tag{4.8}$$

Finally, combining with (4.3), we find

$$I_x = N[P \ \partial/\partial x \ (r \frac{\partial I_x}{\partial x}) + HE_y] \tag{4.9}$$

4.2 Limit of Small Anomalous Resistance

We will examine the structure of these equations by assuming that r may be considered a small perturbation, which probably corresponds to the initial stages of electrojet polarization. In the absence of good information we assume r to be independent of x for simplicity. Since V_{D_i} is proportional to E_x, a small quantity, (4.1b) reduces in steady state and lowest order to

$$N_i(x) = N(x) = \sqrt{\frac{F(x)}{K\alpha h}} \tag{4.10}$$

In lowest order, (4.3) reduces to

$$I_x = N(x) H E_y \tag{4.11}$$

so that $j_{\shortparallel}$ is proportional to the derivative of the ionospheric density, from (4.3),

$$j_{\shortparallel} = - \frac{\partial I_x}{\partial x} = - HE_y \frac{\partial N}{\partial x} \tag{4.12}$$

and the polarization field is proportional to the second derivative of the ionospheric density, from (4.8)

$$E_x = r \frac{\partial^2 I_x}{\partial x^2} = r\, HE_y \frac{\partial^2 N}{\partial x^2} \tag{4.13}$$

We have consistently assumed E_y is independent of x, corresponding to the assumptions that $\underline{E}$ is curl-free and that spatial variations in the east-west y direction may be neglected.

We may now substitute F(x), eq. (3.9), into (4.10-4.13), to find the required spatial dependences:

$$\frac{N(x)}{N(x_T)} = \left(\frac{x}{x_T} \right)^8 \exp \left\{ - \frac{3\delta}{44} \left[\left(\frac{x}{x_T} \right)^{44/3} - 1 \right] \right\} \tag{4.14}$$

$$\frac{J_{\shortparallel}(x)}{J_0} = 8 \left(\frac{x}{x_T} \right)^7 \left[1 - \frac{\delta}{8} \left(\frac{x}{x_T} \right)^{44/3} \right] \exp \left\{ - \frac{3\delta}{44} \left[\left(\frac{x}{x_T} \right)^{44/3} - 1 \right] \right\} \tag{4.15}$$

$$\frac{E_x(x)}{E_0} = 56 \left(\frac{x}{x_T} \right)^6 \left[1 - \frac{89}{168} \delta \left(\frac{x}{x_T} \right)^{44/3} + \frac{\delta^2}{56} \left(\frac{x}{x_T} \right)^{88/3} \right] \cdot \exp \left\{ \frac{-3\delta}{44} \left[\left(\frac{x}{x_T} \right)^{44/3} - 1 \right] \right\} \tag{4.16}$$

where $J_{\shortparallel}(x)$ is the number flux of electrons carrying the parallel current.

(4.14) and (4.15) indicate that the ionospheric density has a single maximum, at $(x/x_T) = (8/\delta)^{3/44}$ of magnitude

$$\frac{N_{max}}{N(x_T)} = (8/\delta)^{6/11} \exp \left\{ \frac{3\delta}{44} - 6/11 \right\} \tag{4.17}$$

Equatorward of the density maximum ($x > x_T(8/\delta)^{3/44}$), $J_{\shortparallel}(x)/J_0$ is negative, which for westward E_y, corresponds to field-aligned currents into the ionosphere, whereas polewards of the density maximum, the field-aligned currents are out of the ionosphere. The current density maxima occur at the zeros of (4.16), or approximately at the points $\delta(x/x_T)^{44/3} \approx 2$ and 88/3. Substituting

into (4.15), we may compare the magnitudes of the poleward $(\delta(x/x_T)^{44/3} \gtrsim 2)$ and equatorward parallel current maxima. The maximum parallel current density into the ionosphere at the equatorward edge of the auroral oval is roughly twice the maximum current density out of the ionosphere poleward of the density maximum. Thus, as E_y increases, the equatorward field-aligned currents will exceed the stability threshold first.

(4.16) indicates the polarization field E_x has two zeroes, at the field-aligned current density maxima. Consequently, this model contains three distinct polarization field regions. At $x/x_T = 1$ and $(x/x_T)^{88/3}$ large, E_x is positive corresponding to northward polarization and eastward electrojet. The middle region, where polarization field is southward and the electrojet westward, corresponds to the normal electrojet.

4.3 Estimate of Physical Magnitudes

We now consider the normalization of $N(x)$, $J_{\parallel}(x)$ and $E_x(x)$ at $x = x_T$, corresponding to the last dipolar field line. Clearly,

$$N(x_T) = \left[\frac{F(x_T)}{k\alpha h}\right]^{1/2} \tag{4.18}$$

whereupon, defining the Hall conductance $\Sigma_H(x_T) = \frac{N(x_T)ec}{B_I} h$ where B_I is the auroral oval magnetic field strength, we find

$$J_0 = \frac{\Sigma_H(x_T)E_y}{e\, x_T} \qquad (el/cm^2\text{-sec}) \tag{4.19}$$

and

$$E_0 = \frac{reJ_0}{x_T} = \frac{r\Sigma_H(x_T)E_y}{x_T^2} \qquad (esu/cm) \tag{4.20}$$

We now estimate the input conditions at $L = L_T(x = x_T)$. The flow solution (3.1) scales with two parameters, L_T and δ; estimating the minimum lifetime to be

$$T_{min} = \frac{\pi L R_E}{a_e} \frac{B_I}{B(L_T)} = \frac{B_I}{B_E} \frac{\pi L^4 R_E}{a_e} \qquad \text{where}$$

B_I/B_E is the ratio of the magnetic field in the auroral oval ionosphere to the equatorial field, R_E is one earth radius, and a_e is the plasma sheet electron thermal speed at $L = L_T$, and scaling the electric field in space E_s to the ionospheric field E_y by the approximate mapping relation,

$$E_s = E_y \left[\frac{B(L_T)}{B_I}\right]^{1/2} = E_y \left[\frac{B_E}{B_I}\right]^{1/2} L_T^{-3/2} \qquad \text{we find}$$

$$\frac{1}{\delta} = \frac{\tilde{L}}{L_T} = \frac{\pi c E_y}{a_e B_I} \left(\frac{B_I}{B(L_T)}\right)^{3/2} = \frac{\pi c E_y}{a_e B_I} \left(\frac{B_I}{B_E}\right)^{3/2} L_T^{9/2} \tag{4.21}$$

We may also scale J_0 and E_0 to the parameters δ and L_T. Using $x_T = R_E L_T^{1/2}$, and (4.21), we find

$$J_0 = \frac{\sum_H(x_T) a_e B_I}{\pi c R_E e} \left(\frac{B_E}{B_I}\right)^{3/2} \frac{1}{\delta L_T^4} \tag{4.22}$$

and

$$E_0 = \frac{r \sum_H(x_T) a_e B_I}{\pi c R_E^2} \left(\frac{B_E}{B_I}\right)^{3/2} \frac{1}{\delta L_T^{7/2}} \tag{4.23}$$

where J_0 has been written in precipitation units. Occasionally, it is convenient to measure $E_x(x)$ in units of the convection field E_y; if $E_x(x)/E_0 = g(x)$ given by eq. (4.16), then

$$\frac{E_x}{E_y} = \frac{gr\Sigma_H(x_T)}{x_T^2} = \frac{gr\Sigma_H(x_T)L_T}{R_E^2} \tag{4.24}$$

In the absence of good models for the inner plasma sheet, we can only make plausible estimates for the quantities (4.18), (4.21-4.24). For example, if we choose the plasma sheet number density $n(L_T) = 0.3/cm^3$, and $T_e(x_T) =$ 1 Kev, then $a_e = 1.33 \times 10^9$ cm/sec and $F(x_T) = 1$ erg/cm^2-sec. Then choosing K = 35 eV/ion pair, h $\approx$ 30 Km, and $\alpha = 2 \times 10^{-7}/cm^6$-sec, we find $N(x_T) = 1.7 \times 10^5/cm^3$. On this basis $\Sigma_H(x_T) = 1.55 \times 10^{13}$ esu $\approx$ 17 mhos. Then using $R_E = 6.4 \times 10^8$ cm, $B_I/B_E = 5/3$ we find

$$\delta = \frac{3.3 \times 10^{-3}}{E_y L_T^{9/2}} \tag{4.25}$$

$$J_0 = \frac{1.6 \times 10^{11}}{L_T^4 \delta} = 5 \times 10^{13} E_y \sqrt{L_T} \tag{4.26}$$

$$E_0 = 1.2 \times 10^{-7} \frac{r}{\delta L_T^{7/2}} \frac{esu}{cm} = \frac{3.6r}{\delta L_T^{7/2}} \frac{mV}{m} \tag{4.27}$$

where E_y is measured in esu/cm.

Assuming a_e does not vary significantly, we can estimate a plausible range for the parameter δ. Let us consider two extreme cases. At quiet times, E_y might be 10 mV/m and $L_T = 10$, whereas during a developed growth phase E_y could increase to 50 mV/m and L_T decrease to 8. For these extremes $\delta = 0.3$ and $\delta = 0.2$. Thus a plausible range of $\delta = 1.0 - 0.1$, for very quiet to very disturbed conditions. Increasing E_y for fixed L_T decreases δ; decreasing L_T increases δ; these two effects tend to compensate each other somewhat in the growth phase. While the shape parameter δ may not vary strongly during growth

phase, equation (4.26) indicates that J_0, which scales the field-aligned current distribution, ought to increase, since E_y increases and $\sqrt{L_T}$ decreases only slightly during growth phase. This indicates that if the field-aligned currents are stable initially, a sufficiently long growth phase will increase them until they become unstable. The scalings (4.25-4.27) do not reflect the fact that $F(x_T)$, and consequently $N(x_T)$ and $\Sigma_H(x_T)$, may also increase due to compression of the plasma sheet. In fact, none of the rough scalings we have been able to deduce contribute to reducing the field-aligned current densities.

4.4 Summary of Results

Figure 1 schematically summarizes the geometrical configuration under consideration. Figures 2, 3 and 4 describe in normalized units the variations of $N(x)$, $J_{\parallel}(x)$, and $E_x(x)$ derived from (4.14-4.16) for various values of δ. δ's of a few tenths seem reasonable. The ionospheric density in Figure 2 rises to an increasingly large and sharp maximum as δ decreases. For $\delta = 0.2$, $N_{max}/N(x_T) \approx 4$, which for $N(x_T) \approx 1.7 \times 10^5/cm^3$ implies $N_{max} \approx 7 \times 10^5/cm^3$, $F_{max} \approx 16$ ergs/cm^2-sec, and $\Sigma_{H(max)} \approx 68$ mhos. The equatorward edge of the auroral oval, defined as the distance over which $N(x)/N(x_T)$ returns to 1, is the order of $0.15\ x_T$, which for $x_T = 2{,}000$ km, is roughly 300 km.

Figure 3 gives the spatial profile of $J_{\parallel}(x)/J_0$ for several values of δ. The region poleward of the density maximum contains positive $J_{\parallel}$ (current out of the ionosphere), and the region equatorward, negative $J_{\parallel}$ (current into the ionosphere). The maximum equatorward $|J_{\parallel}|$ is roughly twice the poleward maximum $|J_{\parallel}|$. We can estimate the threshold convection electric field E_y which will just begin to create anomalous resistance by setting $J_{\parallel(max)}$ equal to 3×10^9 el/cm^2-sec, the rough stability limit calculated by Kindel and

Kennel (1971). With J_0 given by (4.26), $L_T = 9$, $\delta = 0.2$, $J_{\parallel(max)} \approx 30\ J_0$; thus an $E_y \approx 20$ mV/m will begin anomalous resistance and electric field polarization of the ionosphere, in rough agreement with the results of Mozer (1971).

Figure 4 describes the polarization electric field E_x/E_0 assuming a spatially uniform value of r. Actually, r should be small ($E_x \approx 0$) except where $J_\parallel > 3 \times 10^9$ el/cm^2-sec.

We can estimate the anomalous resistance required to polarize the ionosphere, by requiring $|E_x/E_y| \approx O(1)$ the order of magnitude observed by Mozer (1971). For $\delta = 0.2$, g_{max} (eq. 4.24) = 360. For $L_T \approx 10$, $\Sigma_H(x_T) \approx 1.5 \times 10^{13}$, r = 7.4 esu. For this value of r, the maximum potential drop along the field lines, $|\phi_{\parallel(max)}| = |rJ_{\parallel(max)}| \approx 150\ E_y$ volts where E_y is measured in mV/m. For the polarization threshold field, $E_y \approx 20$ mV/m, then $|\phi_{\parallel(max)}|$ is the order of 3 kV.

Figures 5 and 6 plot, for $\delta = 0.2$, $N(x)/N_0$, $J_\parallel(x)/J_0$, the electric field polarization ratio E_x/rE_y, and the total normalized electrojet current $I_y(x)/I_{y0} = \frac{N(x)}{N_0}\left[1 - \frac{\Sigma_H(x_T)}{\Sigma_P(x_T)}\frac{E_x}{E_y}\right]$ where $I_{y0} = \Sigma_H(x_T)E_y$. $\Sigma_H(x_T)/\Sigma_P(x_T)$ has been estimated as 3. In Figure 5, $E_y = 30$ mV/m, and r = 1 was assumed only in the spatial region where $|J_\parallel| > 3 \times 10^9$ el/cm^2-sec; r = 0 outside this region, thus producing the sharp discontinuity in E_x and I_y. Westward electrojet polarization occurs only at the equatorward edge with I_y enhanced by roughly 2 to 4 over its unpolarized level; the electrojet width is roughly 100 km. A very weak eastward electrojet occurs equatorward of the westward electrojet. In Figure 6 $E_y = 50$ mV/m and r = 2 was assumed in the polarization regions ($|J_\parallel| > 3 \times 10^9$ el/cm^2-sec). A strong westward electrojet with I_y enhanced by 2 to 7 times its unpolarized level occurs at the equatorward edge. A weaker westward electrojet also occurs about 150 km. poleward of the equatorward electrojet, since the

outward $J_{\parallel}$ also exceeds the instability threshold. Kisabeth and Rostoker (1971) have observed separate equatorward and poleward electrojets during substorm expansion phase when, presumably, the convection electric field is large. However, the steady state ionospheric density model assumed here is undoubtedly a poor approximation to expansion phase conditions; hence the double electrojet in Figure 6 should be considered as only indicative that multiple polarization and electrojet regions are possible when the field-aligned currents exceed instability threshold.

The detailed variations shown in Figures 5 and 6 are probably not trustworthy, primarily because $E_x(x)$ depends upon the second derivative of the ionospheric density, and ultimately upon that of the plasma sheet heat flux F. Here inaccuracies in the precipitation model are crucial. For example, near the poleward edge ($x \lesssim x_T$), the dipole magnetic field model undoubtedly becomes inaccurate; at the equatorward edge, the precipitation model again becomes questionable, due, for example, to the breakdown of the adiabatic temperature law. Nevertheless, so long as the heat flux into the ionosphere has a maximum, the qualitative features of Figures 4 and 5 should be preserved.

5.0 Discussion

Although strictly speaking the above analysis is severely limited by our assumed ionospheric model, many of its conclusions should have a wider qualitative validity. The electron precipitation heat flux is both observed (Frank and Ackerson, 1971) and theoretically expected (Kennel, 1969) to be spatially inhomogeneous within the nightside auroral oval. The oval ionospheric plasma density should, therefore, have spatial gradients, probably in both latitude and longitude, with our single density maximum model being the simplest possibility. The predominantly westward (near midnight) convection electric field drives a poleward Hall current which, because of the inhomogeneous Hall conductance, cannot be divergence-free in the ionosphere. Longitudinal gradients of the Pedersen conductance will also enhance the Pedersen current divergence. Field-aligned currents must flow into (out of) the ionosphere equatorward (poleward) of any density maximum in order to maintain the total current divergence-free.

Such field-aligned currents may flow freely into space provided that near perfect electrical conduction exists along the field lines. The current circuit is presumably closed via, as yet undetermined, pressure gradient drift currents in the magnetosphere. However, for large convection electric fields and/or sharp ionospheric density gradients, the field-aligned currents can exceed the threshold for instability in the topside ionosphere (Kindel and Kennel, 1971). The unstable plasma turbulence should then produce an anomalous resistance which partially blocks the current. A parallel electric field is then required for the flow of current. Since the Hall current divergnece no longer flows freely, a southward (in the northern hemisphere) polarization electric field develops in the lower ionosphere in order to reduce the Hall current. The coupled convection and polarization electric fields drive a westward Cowling current electrojet which, when Σ_H/Σ_P is large, can greatly

exceed the unpolarized westward current. If several density maxima exist within the oval, and if their associated field-aligned currents are unstable, multiple polarization regions and electrojets should occur.

Although admittedly an idealization, our single density maximum model does delineate several physical trends in the ionospheric response to substorm growth phase. The gradual build-up of the convection electric field (Mozer, 1971) enhances the ionospheric currents (McPherron, 1970) and therefore the field-aligned currents stemming from the divergence of the Hall current. The increased tail flaring stress results in the inward motion of the electron plasma sheet inner edge (Siscoe and Cummings, 1969; Coroniti and Kennel, 1971b), which, since the electrons penetrate deeper into the dipole field, raises the electron precipitation heat flux. The resulting enhancement of the ionospheric conductances further intensifies the field-aligned and ionospheric currents. In our model the sharp inner edge spatial gradient of the precipitation heat flux produces the largest field-aligned currents at the equatorward edge of the auroral oval. Thus, the enhancement of convection, and magnetosphere configurational changes, during growth phase drive the equatorward field-aligned currents toward instability. Even without an impulsive convective collapse of the tail, the field-aligned currents should exceed instability threshold somtime during growth phase provided the convection electric field and ionospheric conductances increase. The subsequent equatorward directed polarization electric field and Cowling current westward electrojet are typical ground-based signatures of substorm expansion phase.

A rapid tail collapse would also drive the field-aligned currents to instability and produce electrojet polarization. Hence there may be two types of substorm breakups: an adiabatic breakup which results solely from the gradual growth phase changes in the magnetosphere; and an impulsive breakup

associated with a rapid convective tail collapse. Carefully timed correlation studies between ground and satellite observations are needed to distinguish whether one or both types of breakup occur.

Semi-quantitative estimates based on the precipitation-ionospheric density model indicate that the typical growth phase westward electric fields of 20-30 mV/m measured by Mozer (1971) are sufficient to produce field-aligned current instability and electrojet polarization at the equatorward edge of the auroral oval. For larger electric fields, $E_y \sim 50$ mV/m, a second westward electrojet may occur one to several hundred kilometers poleward of the equatorward electrojet. From the observed ratio of the polarization to convection electric field $|E_x/E_y| \sim \mathcal{O}(1)$ (Mozer, 1971), the required parallel potential drop across the anomalous resistance region is of order 1-5 kV. The parallel electric field accelerates ions into the ionosphere at the equatorward edge. The anomalous Joule dissipation in the topside ionosphere is of order one erg/cm^2-sec, which is comparable to the total Pedersen dissipation. This represents a non-negligible fraction of the incident electron precipitation heat flux, and could considerably modify the topside ionosphere.

Our simplified precipitation-ionospheric density model is clearly inadequate for expansion phase. First, the structure of auroral arcs and their effects on the ionospheric and field-aligned currents should be included. In fact, recent rocket measurements of large field-aligned currents in arcs (Vondrak, et al., 1971; Park and Cloutier, 1971) indicate that perhaps the entire divergence of the Hall current may flow inside the arcs. Thus arc structure may crucially affect electrojet polarization. Second, as in laboratory experiments, anomalous topside resistance probably produces runaway electrons. At the equatorward edge, runaway electrons are accelerated into space and possibly into the conjugate ionosphere where they may substantially contribute to ionospheric ionization. Since the parallel potentials required

for polarization are of order several kV, the runaway electrons possibly constitute the several keV electron beams often observed during breakup. Third, the anomalous resistance region undoubtedly does not completely prevent the polarization electric field from penetrating into the magnetosphere, as asuumed here. The polarization electric field and any associated field-aligned divergence of the Cowling electrojet into space should modify the convection pattern and the magnetospheric current distribution. Thus, the reaction of the magnetosphere to electrojet polarization needs to be evaluated. Finally, expansion phase is longitudinally asymmetric so that east-west ionospheric density gradients and current divergences must also be considered. Our analysis suggests that when the field-aligned currents are near instability threshold, local measurements of the electric field in the lower ionosphere may not yield an accurate picture of the overall convection pattern, since local ionospheric conductance inhomogeneities will produce local electric field polarizations.

During magnetic storms the plasma sheet inner edge may penetrate far into the dipole and large convection electric fields are expected (Coroniti and Kennel, 1971a,b). Hence $L_T \sim 8$ and $E_y \sim 6 \times 10^{-6}$ esu/cm (the largest polar cap field observed by Cauffman and Gurnett (1971)) might be reasonable; from (4.25) and (4.26) $\delta \gtrsim 0.05$ and $J_0 \gtrsim 8 \times 10^8$ el/cm^2-sec. The field-aligned currents are now unstable nearly everywhere in the oval and electrojet polarization should now occur over virtually the entire nightside auroral oval. Should intense polar cusp precipitation fluxes maintain a very high dayside auroral oval Pedersen conductance during storms (Russell et al., 1971b; Frank, 1971), large electromagnetic inertia of dayside line-tying could then prevent rapid changes in the convection rate (Coroniti and Kennel, 1971a), so that once polarization is established, the nightside oval may remain polarized. Hence

almost continuous electrojet currents might be expected during main phase. The intense Joule dissipation from the field-aligned current instabilities should then greatly modify the structure of the topside ionosphere, and perhaps change the basic physics of ionosphere-magnetosphere interactions.

Acknowledgements

We are pleased to acknowledge useful discussions with F. S. Mozer, R. L. McPherron, J. M. Kindel, M. H. Rees, K. M. Lee, and D. S. Evans. This work was partially supported by the Office of Naval Research, Grant #N00014-69-A-0200-4023; the National Science Foundation, Grant #GP-22817; the Atomic Energy Commission, Contract AT(04-3)-34, Project #157; and the National Aeronautics and Space Administration, Contract NGR-05-007-190 and NGR-05-007-116.

Figure Captions

Figure 1. Schematic of Polarization Model

Light shading illustrates the configuration of plasma sheet electrons in space, bounded at its poleward edge by the last closed field line, and at its equatorward edge by the inner edge of the electron plasma sheet. Dark shading schematically indicates the profile of ionospheric electron density, which should maximize where the plasma sheet electron precipitation flux maximizes. Field-aligned currents surround the ionospheric density maximum. The flow-precipitation coupling model of Section 3 is at best only valid within the last dipolar field line, $L < L_T$; this region maps into the ionosphere as $x > x_T$.

Figure 2. Normalized Ionospheric Electron Density Profiles

Shown here is a variety of ionospheric electron density profiles computed from (4.14) for various values of the convection parameter δ, eq. (3.2). The density $N(x)$ is normalized to $N(x_T)$, the electron density produced by the plasma sheet electron heat flux at $x = x_T$. All distances x are normalized to x_T, the distance from the geomagnetic pole of the last dipolar field line. If the last dipolar line corresponds to 20° colatitude, then $x_T \simeq 2{,}000$ km. δ of a few tenths seems reasonable. Consequently the ionospheric density increases by a factor 2-4 in a few hundred kilometers and then diminishes rapidly. This density variation could be difficult to observe directly.

Figure 3. Normalized Field-Aligned Current Density Profiles

The field-aligned current densities computed from Eq. (4.15) are plotted for various values of δ, eq. (3.2). The field-aligned current density maximizes at the points of maximum ionospheric density gradient. For the single density maximum models of Figure 2, a westward electric field creates currents into the ionosphere equatorward, and out poleward, of the density maximum. When the density profile is asymmetric, with a sharp equatorward gradient, the equatorward field-aligned current density maximum is larger than the poleward maximum, in absolute magnitude. For this configuration, the equatorward field-aligned currents should reach instability first as the convection field increases.

Figure 4. Normalized Polarization Electric Fields

Assuming the anomalous resistance r is nonzero and uniform throughout the oval, the above polarization electric field profiles result. The polarization electric field changes sign at each field-aligned current maximum. An equatorward electric field, leading to a westward electrojet, lies between the two current maxima. On either side is a poleward polarization field.

Figure 5. Single Auroral Electrojet

Here we substitute a value of the auroral oval electric field, 30 mV/m, in order to estimate the region where $|J_{\parallel}|$ exceeds the stability limits calculated by Kindel and Kennel, 1971. The unstable region is shaded in the middle curve of field-aligned current. In addition, the anomalous resistance r is taken nonzero only in the unstable region. This produces the electrojet profile shown in the bottom curve. Even though the polarization electric field (dotted curve in middle) magnitudes are comparable in the eastward and westward electrojet, the westward electrojet is more

intense, because it falls in a region of higher ionospheric electron density. For x_T = 2,000 km, the westward electrojet is roughly 100 km thick. The ionospheric density profile is shown at the top for reference.

Figure 6. Double Auroral Electrojet

For a westward electric field of 50 mV/m, both field-aligned current maxima can be unstable, producing twin electrojet pairs. In each case, the westward electrojet is the stronger. The two electrojet pairs are separated by the order of 100 km.

References

Arnoldy, R.L., "Signature of the interplanetary medium for substorms," J. Geophys. Res., 76, 5189, 1971.

Aubry, M.P., C.T. Russell and M.G. Kivelson, "On inward motion of the magnetopause preceeding a substorm," J. Geophys. Res., 75, 7018, 1970.

Aubry, M.P. and R.L. McPherron, "Magnetotail changes in relation to the solar wind magnetic field and magnetospheric substorms," J. Geophys. Res. 76, 4381, 1971.

Axford, W.K., H.E. Petschek, and G.L. Siscoe, "Tail of the magnetosphere," J. Geophys. Res., 70, 1231, 1965.

Bostrom, R., "A model of the auroral electrojet," J. Geophys. Res., 69, 4983, 1964.

Camidge, F.P. and G. Rostoker, "Magnetic field perturbations in the magnetotail associated with polar magnetic substorms," Can. J. Phys., 48, 2002, 1970.

Cauffman, D.P. and D.A. Gurnett, "Double-probe measurements of convection electric fields with the Injun-5 satellite," J. Geophys. Res., 76, 6014, 1971.

Coroniti, F.V. and C.F. Kennel, "Magnetopause motions, DP-2, and the growth phase of magnetospheric substorms," Submitted to J. Geophys. Res., 1971.

Coroniti, F.V. and C.F. Kennel, "Changes in magnetospheric configuration during substorm growth phase," Submitted to J. Geophys. Res., 1972.

Dungey. J.W., "Interplanetary magnetic field and the auroral zones," Phys. Rev. Letters, 6, 47, 1961.

Evans, D.S., "The observations of a near monoenergetic flux of auroral electrons," J. Geophys. Res., 73, 2315, 1968.

Fairfield, D.G. and L.J. Cahill, "Transition region magnetic field and polar magnetic disturbances," J. Geophys. Res., 71, 155, 1966.

Fairfield, D.H. and N.F. Ness, "Configuration of the geomagnetic tail during substorms," J. Geophys. Res., 75, 7032, 1970.

Frank, L.A. and K.L. Ackerson, "Observations of charged particle precipitation into the auroral zone," J. Geophys. Res., 76, 3612, 1971.

Frank, L.A., Plasma in the earth's polar magnetosphere," J. Geophys. Res., 76, 5202, 1971.

Fukushima, N., "Equivalence in ground geomagnetic effect of Chapman-Vestine's and Birkeland-Alfven's electric current-systems for polar magnetic storms," Rep. Ionos. Space Res. Japan, 23, 219, 1969b.

Hamberger, S.M. and J. Jancarik, "Experimental studies of electrostatic fluctuations in a turbulently heated plasma," To be published, Physics of Fluids, 1972.

Heppner, J.P., J.D. Stolarik, and E.M. Wescott, "Electric-field measurements and the identification of currents causing magnetic disturbances in the polar cap," J. Geophys. Res., 76, 6028, 1971.

Hirshberg, J. and D.S. Colburn, "Interplanetary field and geomagnetic variations: a unified view," Planet. Space Sci., 17, 1183, 1969.

Hones, E.W. Jr., "Magnetotail plasma and magnetospheric substorms," in Particles and Fields in the Magnetosphere (Ed. by B.M. McCormac), p. 24-33, D. Reidel Publishing Co., Dordrecht-Holland, 1970.

Hones, E.W., J.R. Asbridge, and S.J. Bame, "Time variations of the magnetotail plasma sheet at 18 R_E determined from concurrent observations by a pair of Vela satellites," J. Geophys. Res., 76, 4402, 1971.

Levy, R.H., H.E. Petschek, and G.L. Siscoe, "Aerodynamic aspects of the magnetospheric flow," AIAAJ., 2, 2065, 1964.

Kennel, C.F., "Consequences of a magnetospheric plasma," Rev. of Geophysics, 7, 379, 1969.

Kindel, J.M. and C.F. Kennel, "Topside current instabilities," J. Geophys. Res., 76, 3055, 1971.

Kisabeth, J.L. and G. Rostoker, "Development of the polar electrojet during polar magnetic substorms," J. Geophys. Res., 76, 6815, 1971.

McPherron, R.L., "Growth phase of magnetospheric substorms," J. Geophys. Res., 75, 5592, 1970.

Mozer, F.S. and P. Bruston, "Electric field measurements in the auroral ionosphere," J. Geophys. Res., 72, 1109, 1967.

Mozer, F.S. and R. Manka, "Magnetospheric electric field properties deduced from simultaneous balloon flights," J. Geophys. Res., 76, 1967, 1971.

Mozer, F.S., "The origin and effects of electric fields during isolated magnetospheric substorms," J. Geophys. Res., 76, 7595, 1971.

Nishida, A., "Geomagnetic DP-2 fluctuations and associated magnetospheric phenomena," J. Geophys. Res., 73, 1795, 1968.

Nishida, A., "Coherence of geomagnetic DP-2 fluctuations wthh interplanetary magnetic field variations," J. Geophys. Res., 73, 5549, 1968.

Nishida, A., "DP-2 and polar substorms," Planet. Space Sci., 19, 205, 1971.

Oguti, T., "Development and decay of minor polar geomagnetic disturbances," Rep. Ionos. Space Res., Japan, 22, 25, 1968.

Park, R.J. and P.A. Cloutier, "Rocket-based measurement of Birkeland currents related to an auroral arc and electrojet," J. Geophys. Res., 76, 7714, 1971

Rees, M.H., "Auroral ionization and excitation by incident energetic electrons," Planet. Space Sci., 11, 1209, 1963.

Russell, C.T., R.L. McPherron and P.J. Coleman, "Magnetic field variations in the near geomagnetic tail associated with weak substorm activity," J. Geophys. Res., 76, 1823, 1971.

Russell, C.T., C.R. Chappell, M.D. Montgomery, M. Neugebauer, and F.L. Scarf, "Ogo 5 observations of the polar cusp on Nov. 1, 1968," J. Geophys. Res., 76, 6743, 1971.

Siscoe, G.L. and W.D. Cummings, "On the cause of geomagnetic bays," Planet. Space Sci., 17, 1795, 1969.

Vasyliunas, V.M., "A survey of low energy electrons in the evening sector of the magnetosphere with OGO 1 and OGO 3," J. Geophys. Res., 73, 2839, 1968.

Vondrak, R.R., H.R. Anderson and R.J. Spiger, "Rocket-based measurement of particle fluxes and currents in an auroral arc," J. Geophys. Res., 76, 7701, 1971.

Zmuda, A.J., F.T. Heuring and J.G. Martin, "Dayside magnetic disturbances at 1100 kilometers in the auroral oval," J. Geophys. Res., 72, 1115, 1967.

Zmuda, A.J., J.C. Armstrong, F.T. Heuring, "Characteristics of transverse magnetic disturbances observed at 1100 kilometers in the auroral oval," J. Geophys. Res., 75, 4757, 1970.

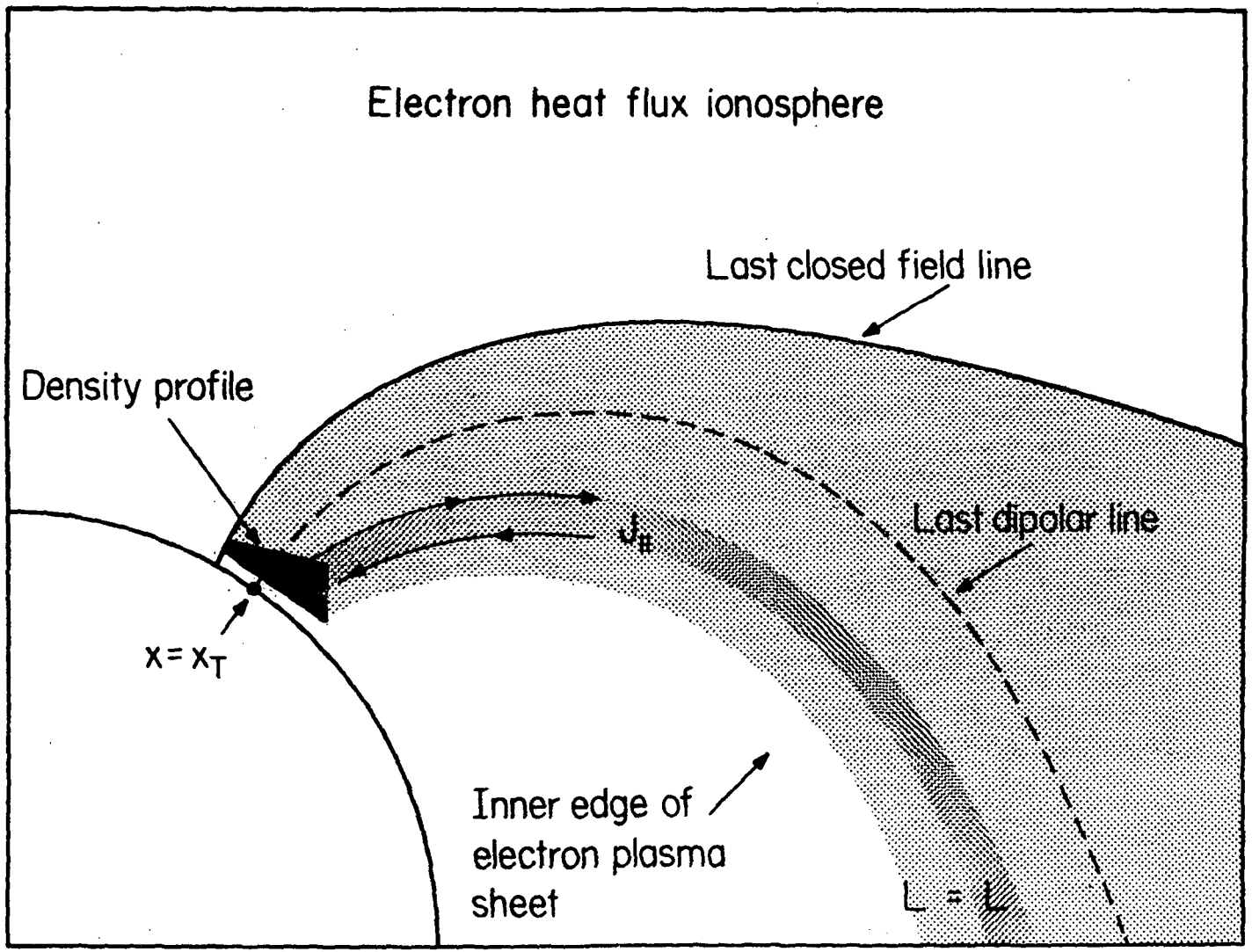
Electron heat flux ionosphere
Last closed field line
Density profile
$J_{\#}$
Last dipolar line
$x = x_T$
Inner edge of
electron plasma
sheet
$L = L$

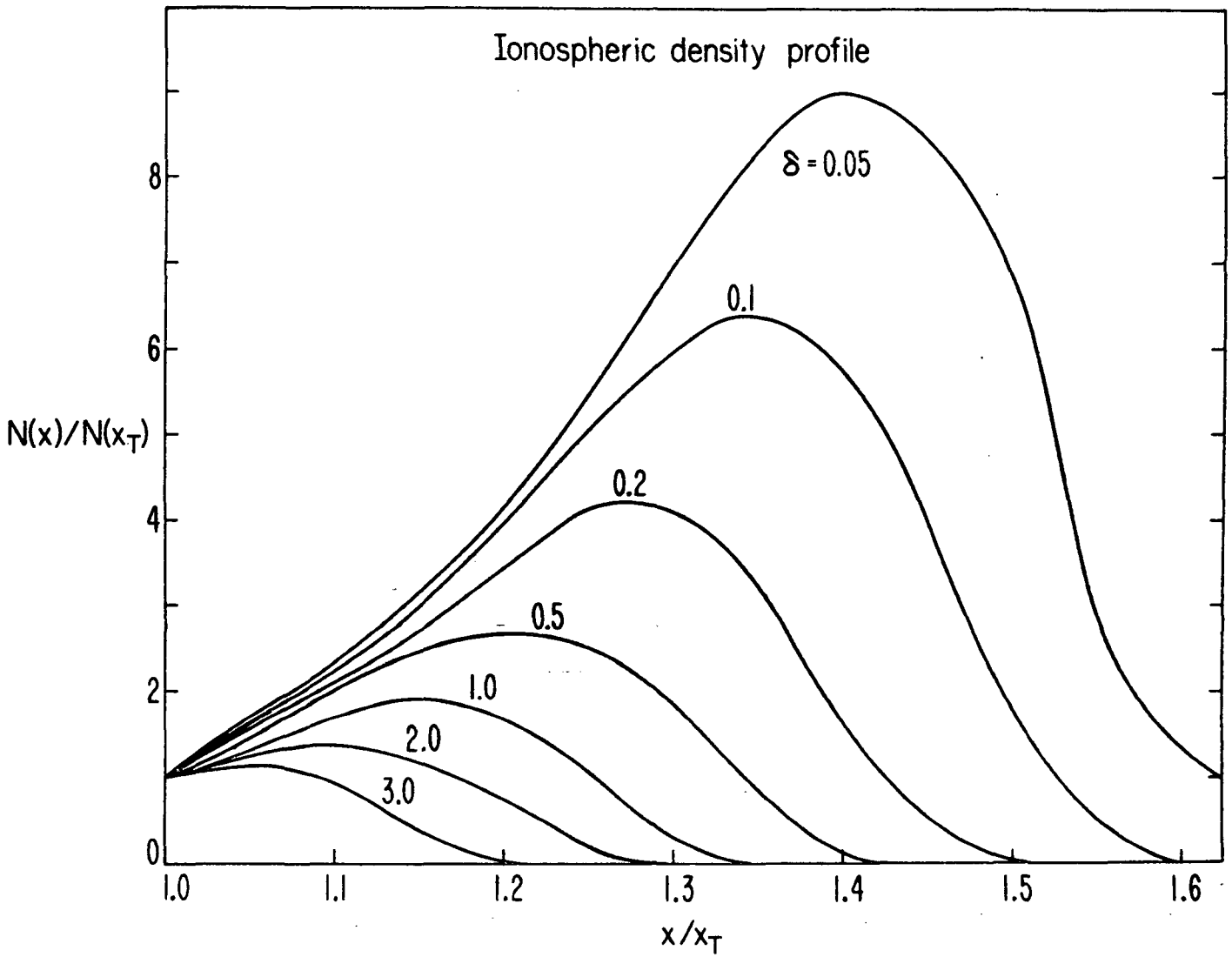
Ionospheric density profile
δ = 0.05
0.1
0.2
0.5
1.0
2.0
3.0
N(x)/N(x_T)
x/x_T
0
2
4
6
8
1.0
1.1
1.2
1.3
1.4
1.5
1.6

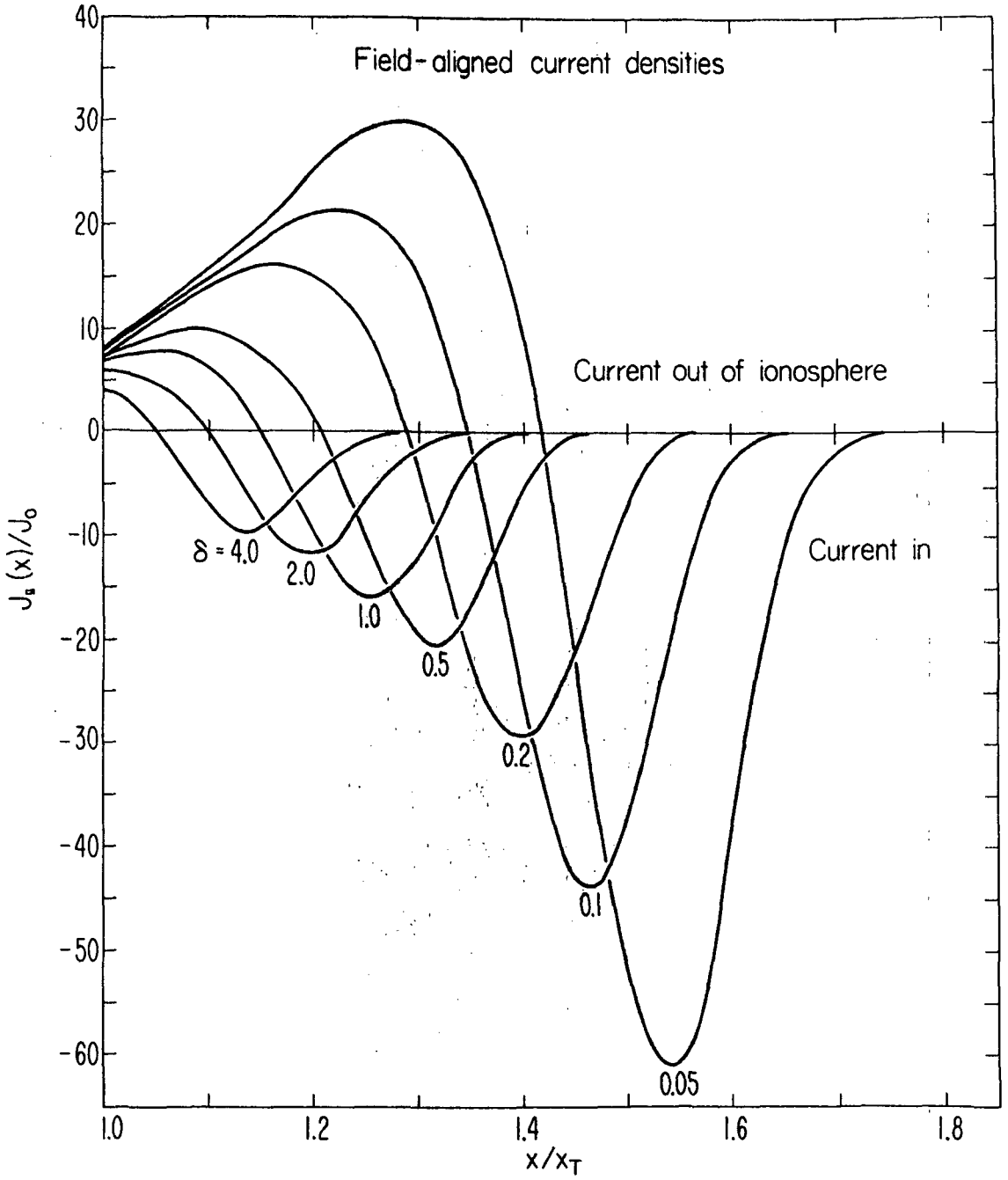
Field-aligned current densities
Current out of ionosphere
Current in
δ = 4.0
2.0
1.0
0.5
0.2
0.1
0.05
40
30
20
10
0
-10
-20
-30
-40
-50
-60
1.0
1.2
1.4
1.6
1.8
$J_s(x)/J_o$
x/x_T

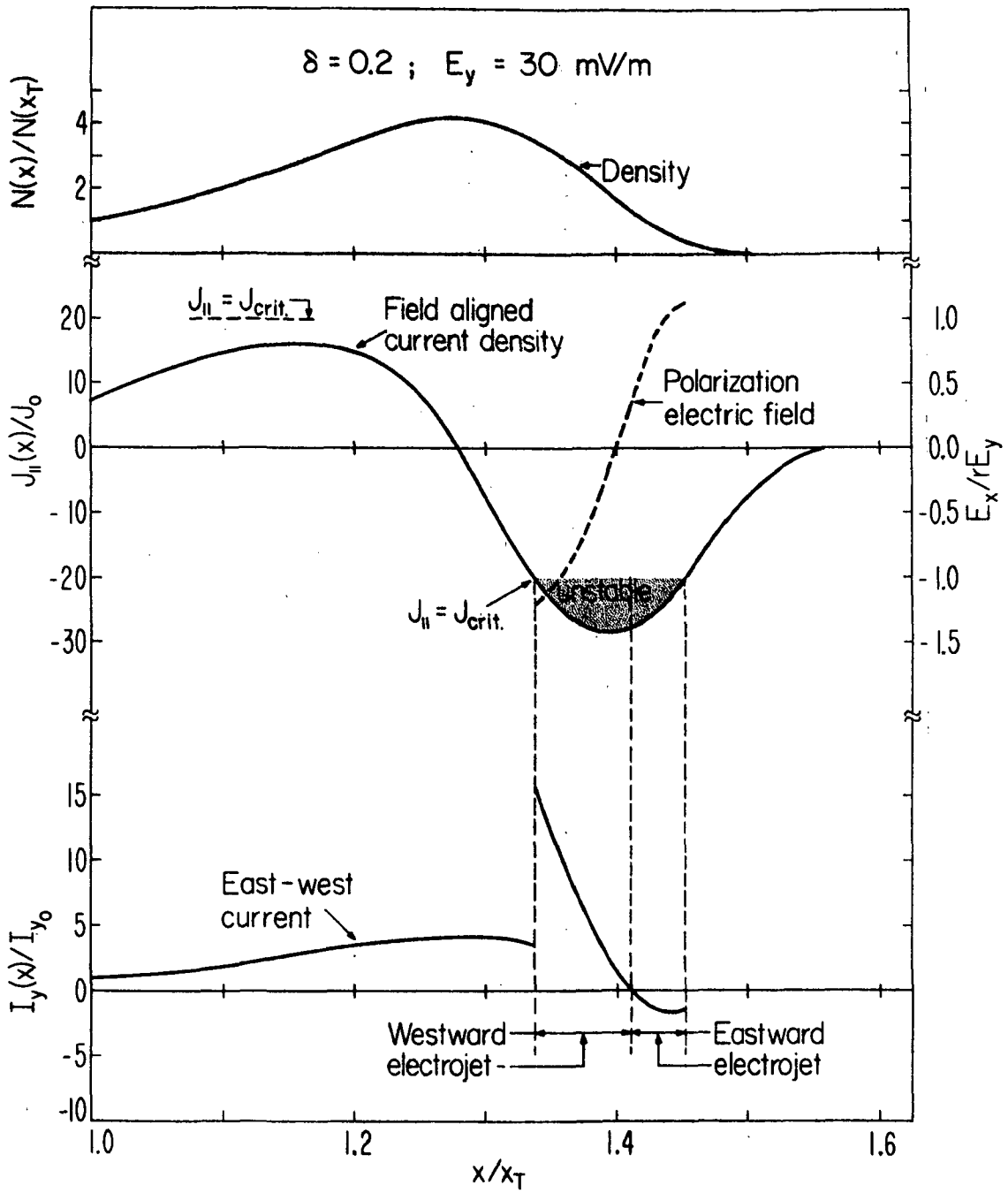
δ = 0.2 ; E_y = 30 mV/m
N(x)/N(x_T)
Density
J_∥ = J_crit.
Field aligned current density
Polarization electric field
J_∥(x)/J_o
E_x/rE_y
Unstable
J_∥ = J_crit.
East-west current
I_y(x)/I_yo
Westward electrojet
Eastward electrojet
x/x_T

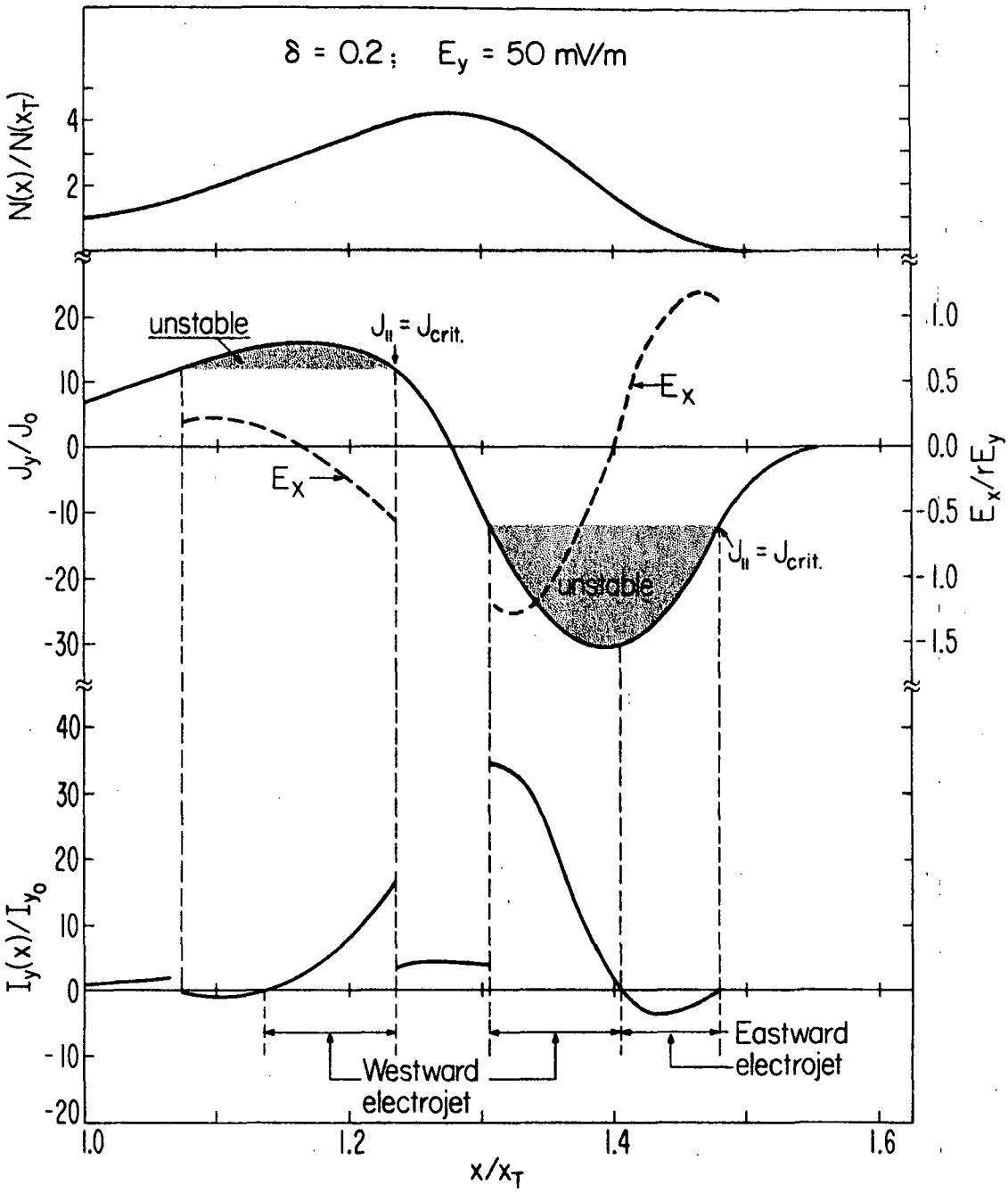
δ = 0.2; Ey = 50 mV/m
N(x)/N(xT)
unstable
J|| = Jcrit.
Ex
Jy/Jo
Ex/rEy
unstable
J|| = Jcrit.
Iy(x)/Iyo
Eastward electrojet
Westward electrojet
x/xT

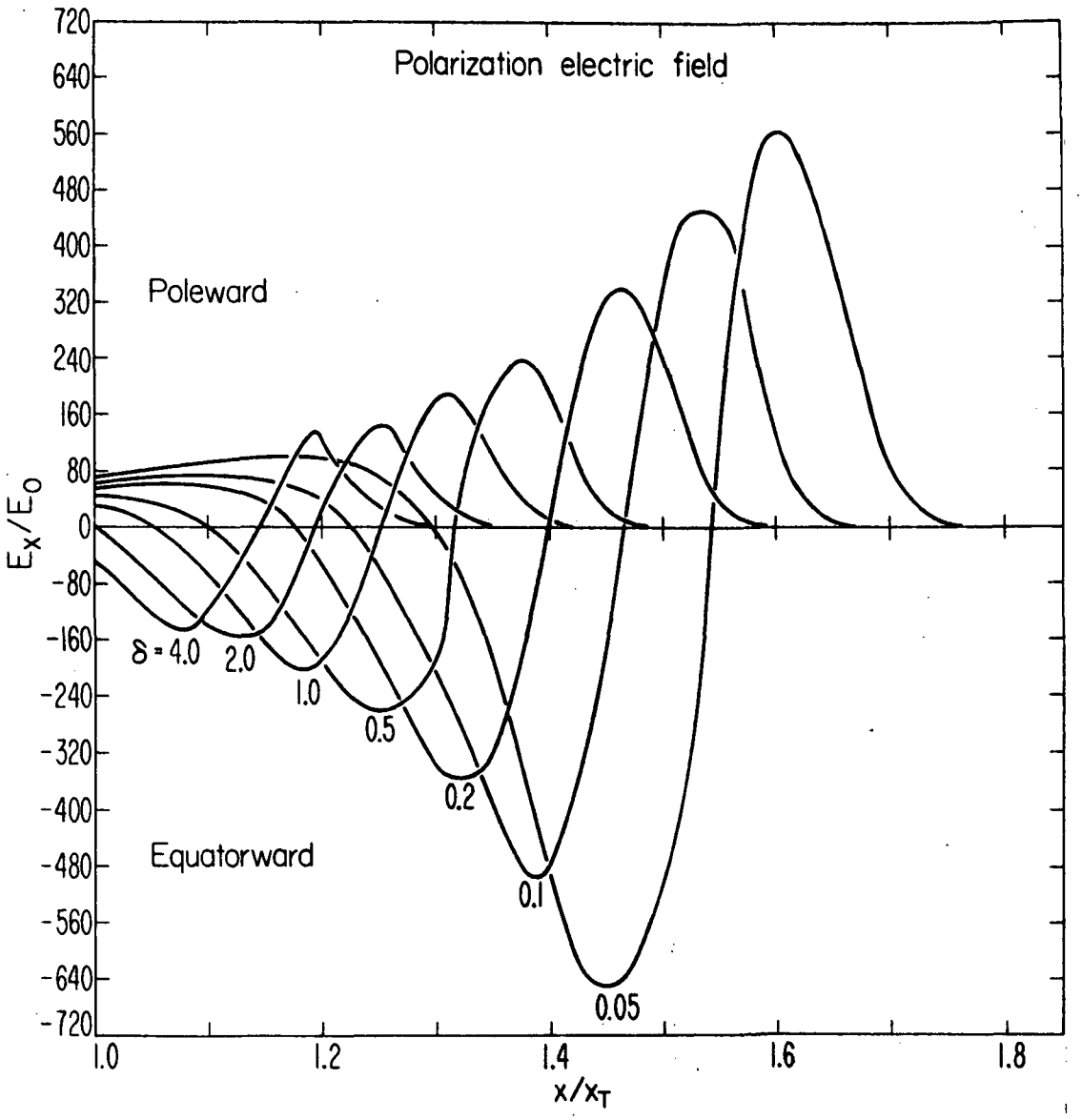
Polarization electric field
Poleward
Equatorward
δ = 4.0
2.0
1.0
0.5
0.2
0.1
0.05
720
640
560
480
400
320
240
160
80
0
-80
-160
-240
-320
-400
-480
-560
-640
-720
1.0
1.2
1.4
1.6
1.8
E_x/E_0
x/x_T

UCLA PLASMA PHYSICS GROUP REPORTS

R-1 "Propagation of Ion Acoustic Waves Along Cylindrical Plasma Columns", A.Y. Wong (**July 1965**)

R-2 "Stability Limits for Longitudinal Waves in Ion Beam-Plasma Interaction", B.D. Fried and A.Y. Wong (August 1965)

R-3 "The Kinetic Equation for an Unstable Plasma in Parallel Electric and Magnetic Fields", B.D. Fried and S.L. Ossakow (Nov. 1965)

R-4 "Low-Frequency Spatial Response of a Collisional Electron Plasma", B.D. Fried, A.N. Kaufman and D.L. Sachs (Aug. 1965)

R-5 "Effects of Collisions on Electrostatic Ion Cyclotron Waves", A.Y. Wong, O. Judd and F. Hai (Dec. 1965)

R-6 "Interaction Between Ion Beams and Plasmas", R. Rowberg, A.Y. Wong and J.M. Sellen (April 1966)

R-7 "Observation of Cyclotron Echoes from a Highly Ionized Plasma", D.E. Kaplan and R.M. Hill (May 1966)

R-8 "Excitation and Damping of Drift Waves", A.Y. Wong and R. Rowberg (July 1966)

R-9 "The Guiding Center Approximation in Lowest Order", Alfredo Banos, Jr. (Sept. 1966)

R-10 "Plasma Streaming into a Magnetic Field", S.L. Ossakow (Nov. 1966)

R-11 "Cooperative Effects in Plasma Echo Phenomena", A.Y. Wong (March 1967)

R-12 "A Quantum Mechanical Study of the Electron Gas Via the Test Particle Method", M.E. Rensink (March 1967)

R-13 "Linear and Nonlinear Theory of Grid Excitation of Low Frequency Waves in a Plasma", G.L. Johnston (April 1967)

R-14 "The Expansion and Diffusion of an Isolated Plasma Column", J. Hyman (May 1967)

R-15 "Two-pole Approximation for the Plasma Dispersion Function", B.D. Fried, C.L. Hedrick and J. McCune (August 1967)

R-16 "Experimental Investigation of Electron Runaway Phenomena", J.S. DeGroot (August 1967)

R-17 "Parametric Coupling Between Drift Waves", F. Hai, R. Rowberg and A.Y. Wong (Oct. 1967)

R-18 "Cyclotron Echoes from Doppler Effects", A.Y. Wong (March 1968)

R-19 "Ion Wave Echoes", D.R. Baker, N.R. Ahren and A.Y. Wong (Nov. 1967)

R-20 "Cyclotron Echoes in Plasmas", O. Judd, Thesis (March 1968)

R-21 "Test Particle Theory for Quantum Plasmas", M.E. Rensink (Oct. 1967)

R-22 "Artificial Van Allen Belt", Charles F. Kennel (Nov. 1967)

R-23 "Landau Damping of Ion Acoustic Waves in a Cesium Plasma with Variable Electron-Ion Temperature Ratio, K.B. Rajangam (Oct. 1967)

R-24 "The Inhomogeneous Two-Stream Instability", G. Knorr (Sept. 1967)

R-25 "Magnetic Turbulence in Shocks", C.F. Kennel and H.E. Petschek (Dec. 1967)

R-26 "Small Amplitude in High Beta Plasmas", V. Formisano and C. Kennel (Feb. 1968)

R-27 "Low Beta Plasma Penetration Across a Magnetic Field", B.D. Fried and S. Ossakow (March 1968)

R-28 "Annual Status Report", Feb. 1, 1967-Jan. 31, 1968, Principal Investigators A. Banos, Jr., B.D. Fried, C.F. Kennel

R-29 "The Theorist's Magnetosphere", C. Kennel (April 1968)

R-30 "Electromagnetic Pitch Angle Instabilities in Space", C.F. Kennel and F.L. Scarf (April 1968)

R-31 "Electromagnetic Echoes in Collisionless Plasmas," A.Y. Wong (April 1968)

R-32 "Parametric Excitation of Drift Waves in a Resistive Plasma", G. Weyl and M. Goldman (June 1968)

R-33 "Parametric Excitation from Thermal Fluctuations at Plasma Drift Wave Frequencies", A.Y. Wong, M.V. Goldman, F. Hai, R. Rowberg (May 1968)

R-34 "Current Decay in a Streaming Plasma Due to Weak Turbulence ", S.L. Ossakow and B.D. Fried (June 1968)

R-35 "Temperature Gradient Instabilities in Axisymmetric Systems", C.S.Liu (August 1968)

R-36 "Electron Cyclotron Echo Phenomena in a Hot Collisionless Plasma", O. Judd (August 1968)

R-37 "Transverse Plasma Wave Echoes", B.D. Fried and Craig Olson (Oct. 1968)

R-38 "Low Frequency Interchange Instabilities of the Ring Current Belt", C.S. Liu (Jan. 1969)

R-39 "Drift Waves in the Linear Regime", R.E. Rowberg and A.Y. Wong (Feb. 1969)

R-40 "Parametric Mode-Mode Coupling Between Drift Waves in Plasmas", F. Hai and A.Y. Wong (Jan. 1969)

R-41 "Nonlinear Oscillatory Phenomena with Drift Waves in Plasmas", F. Hai and A.Y. Wong (Sept. 1960)

R-42 "Ion-Burst Excited by a Grid in a Plasma", H. Ikezi and R.J. Taylor (Feb. 1969)

R-43 "Measurements of Diffusion in Velocity Space from Ion-Ion Collisions", A. Wong and D. Baker (March 1969)

R-44 "Nonlinear Excitation in the Ionosphere", A.Y. Wong (March 1969)

R-45 "Observation of First-Order Ion Energy Distribution in Ion Acoustic Waves, H. Ikezi and R. Taylor (March 1969)

R-46 "A New Representative for the Conductivity Tensor of a Collisionless Plasma in a Magnetic Field", B.D. Fried and C. Hedrick (March 1969)

R-47 "Direct Measurements of Linear Growth Rates and Nonlinear Saturation Coefficients", F. Hai (April 1969)

R-48 "Electron Precipitation Pulsations", F. Coroniti and C.F. Kennel (April 1969)

R-49 "Auroral Micropulsation Instability", F. Coroniti and C.F. Kennel (May 1969)

R-50 "Effect of Folker-Plank Collisions on Plasma Wave Echoes", G. Johnston (June 1969)

R-51 "Linear and Nonlinear Theory of Grid Excitation of Low Frequency Waves in a Plasma", G. Johnston (July 1969)

R-52 "Theory of Stability of Large Amplitude Periodic (BGK) Waves in Collisionless Plasmas", M.V. Goldman (June 1969)

R-53 "Observation of Strong Ion Wave-Wave Interaction", R. Taylor and H. Ikezi (August 1969)

R-55 "Optical Mixing in a Magnetoactive Plasma", G. Weyl (August 1969)

R-56 "Trapped Particles and Echoes", A.Y. Wong and R. Taylor (Oct. 1969)

R-57 "Formation and Interaction of Ion-Acoustic Solitons", H. Ikezi, R.J. Taylor and D.R. Baker (July 1970)

R-58 "Observation of Collisionless Electrostatic Shocks", R. Taylor, D. Baker and H. Ikezi (Dec. 1969)

R-59 "Turbulent Loss of Ring Current Protons", J.M. Cornwall, F.V. Coroniti and R.M. Thorne (Jan. 1970)

R-60 "Efficient Modulation Coupling Between Electron and Ion Resonances in Magnetoactive Plasmas", A. Wong, D.R. Baker, N. Booth (Dec. 1969)

R-61 "Interaction of Quasi-Transverse and Quasi-Longitudinal Waves in an Inhomogeneous Vlasov Plasma", C.L. Hedrick (Jan.1970)

R-62 "Observation of Strong Ion-Acoustic Wave-Wave Interaction", R.J. Taylor and H. Ikezi (Jan. 1970)

R-63 "Perturbed Ion Distributions in Ion-Waves and Echoes", H. Ikezi and R. Taylor (Jan. 1970)

R-64 "Propagation of Ion Cyclotron Harmonic Wave", E.R. Ault and H. Ikezi (Nov. 1970)

R-65 "The Analytic and Asymptotic Properties of the Plasma Dispersion Function", A. Banos, Jr. and G. Johnston (Feb. 1970)

R-66 "Effect of Ion-Ion Collision and Ion Wave Turbulence on the Ion Wave Echo", Dan Baker (June 1970)

R-67 "Dispersion Discontinuities of Strong Collisionless Shocks", F.V. Coroniti (March 1970)

R-68 "An Ion Cyclotron Instability", E.S. Weibel (April 1970)

R-69 "Turbulence Structure of Finite-Beta Perpendicular Fast Shocks", F.V. Coroniti (April 1970)

R-70 "Steepening of Ion Acoustic Waves and Formation of Collisionless Electrostatic Shocks", R. Taylor (April 1970)

R-71 "A Method of Studying Trapped Particles Behavior in Magnetic Geometries:, C.S. Liu and A.Y. Wong (April 1970)

R-72 "A Note on the Differential Equation $g'' + x^2 g = 0$", E.S. Weibel (April 1970)

R-73 "Plasma Response to a Step Electric Field Greater than the Critical Runaway Field, With and Without an Externally Applied Magnetic Field", J.E. Robin (June 1970)

R-74 "The UC Mathematical On-Line Systems as a Tool for Teaching Physics", B.D. Fried and R. White (August 1970)

R-75 "High Frequency Hall Current Instability", K. Lee, C.F. Kennel, J.M. Kindel (August 1970)

R-76 "Laminar Wave Train Structure of Collisionless Magnetic Slow Shocks", F.V. Coroniti (Sept. 1970)

R-77 "Field Aligned Current Instabilities in the Topside Ionosphere", J.M. Kindel and C.F. Kennel (Aug. 1970)

R-78 "Spatial Cyclotron Damping", Craig Olson (September 1970)

R-79 "Electromagnetic Plasma Wave Propagation Along a Magnetic Field", C.L. Olson (September 1970)

R-80 "Electron Plasma Waves and Free-Streaming Electron Bursts", H. Ikezi, P.J. Barrett, R.B. White and A.Y. Wong (Nov. 1970)

R-81 "Relativistic Electron Precipitation During Magnetic Storm Main Phase", R.M. Thorne and C.F. Kennel (Nov. 1970)

R-82 "A Unified Theory of SAR Arc Formation at the Plasmapause", J.M.Cornwall, F.V. Coroniti and R.M. Thorne (Nov. 1970)

R-83 "Nonlinear Collisionless Interaction between Electron and Ion Modes in Inhomogeneous Magnetoactive Plasmas", N. Booth (Dec. 1970)

R-85 "Remote Double Resonance Coupling of Radar Energy to Ionospheric Irregularities", C.F. Kennel (Jan. 1971)

R-86 "Ion Acoustic Waves in a Multi-ion Plasma", B.D. Fried, R. White, T. Samec (Jan. 1971)

R-87 "Current-Driven Electrostatic and Electromagnetic Ion Cyclotron Instabilities," D.W. Forslund, C.F.Kennel, J. Kindel (Feb. 1971)

R-88 "Locating the Magnetospheric Ring Current", C.F. Kennel and Richard Thorne (March, 1971).

R-89 "Ion Acoustic Instabilities Due to Ions Streaming Across Magnetic Field", P.J. Barrett, R.J. Taylor (March, 1971)

R-90 "Evolution of Turbulent Electronic Shocks", A.Y. Wong, R. Means (July, 1971)

R-91 "Density Step Production of Large Amplitude Collisionless Electrostatic Shocks and Solitons", David B. Cohen (June, 1971)

R-92 "Turbulent Resistivity, Diffusion and Heating", Burton D. Fried, Charles F. Kennel, et al. (June, 1971)

PPG-93 "Nonlinear Evolution and Saturation of an Unstable Electrostatic Wave", B.D. Fried, C.S. Liu, et al. (August, 1971)

PPG-94 "Cross-field Current-driven Ion Acoustic Instability", P.J. Barrett, B.D. Fried, C.F. Kennel, J.M. Sellen, and R.J. Taylor (December, 1971)

R-95 "3-D Velocity Space Diffusion in Beam-Plasma Interaction without Magnetic Field", P.J. Barrett, D. Gresillon and A.Y. Wong (September, 1971)

PPG-96 "Dayside Auroral Oval Plasma Density and Conductivity Enhancements due to Magnetosheath Electron Precipitation", C.F. Kennel and M.H. Rees (September, 1971)

PPG-97 "Collisionless Wave-particle Interactions Perpendicular to the Magnetic Field", A.Y. Wong, D.L. Jassby (September, 1971)

PPG-98 "Magnetospheric Substorms", F.V. Coroniti and C.F. Kennel (September, 1971)

PPG-99 "Magnetopause Motions, DP-2, and the Growth Phase of Magnetospheric Substorms", F.V. Coroniti and C.F.Kennel (September, 1971)

PPG-100 "Structure of Ion Acoustic Solitons and Shock Waves in a Two-Component Plasma", R.B. White, B.D. Fried, F.V. Coroniti (September, 1971)

PPG-101 "Solar Wind Interaction with Lunar Magnetic Field", G. Siscoe (Meteorology Dept.) and Bruce Goldstein (JPL) November, 1971

PPG-102 "Changes in Magnetospheric Configuration During Substorm Growth Phase", F.V. Coroniti and C.F. Kennel (November,1971)

PPG-103 "Trip Report - 1971 Kiev Conference on Plasma Theory and Visits to Lebedev and Kurchatov Institutes", B.D. Fried (October, 1971)

PPG-104 "Pitch Angle Diffusion of Radiation Belt Electrons within the Plasmasphere", Lawrence R. Lyons, Richard M. Thorne, Charles F. Kennel (January, 1972)

PPG-105 "Remote Feedback Stabilization of a High-Beta Plasma", Francis F. Chen, Daniel Jassby and M. Marhik, January, 1972